Individual isotopic fragmentation cross sections of relativistic nuclei in hydrogen, helium, and carbon targets

W. R. Webber, J. C. Kish, and D. A. Schrier
Space Science Center, University of New Hampshire, Durham, New Hampshire 03824
(Received 30 December 1988)

In this paper, the third in a series of papers, we discuss isotopic fragmentation cross sections measured in hydrogen, helium, and carbon targets. Over 300 of these cross sections have been measured in 24 separate runs using 12 charges from ^{12}C to ^{58}Ni. Most of these isotope cross sections were measured at an energy ~600 MeV/nucleon, however, some measurements of the ^{56}Fe fragmentation are available at an energy $\gtrsim$ 1 GeV/nucleon. We observe, comparing both these data and other data, that to first order, the mass fractions for each isotope are essentially independent of energy. This indicates that the energy dependence of the isotopic cross sections is essentially the same as for the charge changing cross sections. It is also observed that the isotopic mass fractions and the width of the mass distributions for each charge are essentially independent of the H, He, and C targets involved. These systematics greatly simplify the construction of a semiempirical formula to describe these cross sections. New isotopic cross sections are presented for a number of interesting reactions, ^{12}C→Be, ^{16}O→N, ^{27}Al→Na, and ^{56}Fe into Mn and Ar among others. A large body of new data on proton and neutron stripping reactions are also presented and discussed.

I. INTRODUCTION

This is the third in a series of papers dealing with the cross sections measured using ^{12}C, ^{14}N, ^{16}O, ^{20}Ne, ^{24}Mg, ^{27}Al, ^{28}Si, ^{32}S, ^{40}Ar, ^{40}Ca, ^{56}Fe, and ^{58}Ni beams with energies between 300 and 1700 MeV/nucleon incident on hydrogen (CH_2), carbon, and helium targets at the Lawrence Berkeley Laboratory Bevalac. In this paper we will discuss the individual isotopic cross sections of the fragments. This work is part of a systematic study of the individual elemental and isotopic cross sections in hydrogen and helium targets, appropriate to the interpretation of the interstellar production of secondary fragments by cosmic rays propagating through the galaxy in order to determine the source elemental and isotopic composition of cosmic rays. At the same time it should be noted that the basic systematics of these isotopic cross sections as a function of incident charge, charge change, and target are an important input for understanding the nuclear physics involved in these collisions.

The basic details of the runs, covering studies at the Bevalac, with a total of 42 separate beams of the 12 charges listed earlier, are described in papers I and II.[1,2] In this paper we will discuss the individual isotopic cross sections obtained. These are obtained using the Cerenkov x total energy technique of mass analysis in the isotope module of our telescope. Because of the limitations of this technique these isotopic measurements do not cover as extensive a range in energy or fragment charge as the elemental cross sections reported in paper II. They form, however, the most extensive set of isotopic cross sections of relativistic nuclei presently available. These new cross sections will be compared with other measurements of isotopic cross sections reported in the literature. These other measurements have been made primarily using energetic protons incident on various targets, with the subsequent measurement of the decay of the radioactive isotopes produced. In addition a complete set of isotopic cross sections from ^{12}C and ^{16}O fragmentation at energies ~2 GeV/nucleon is available from Bevalac studies, Lindstrom *et al.*[3] and Olsen *et al.*[4]

II. THE EXPERIMENT AND THE MEASUREMENT TECHNIQUE

The general properties of the experimental set up have been described in paper I of this series. Here we discuss the features of the experiment appropriate to the determination of the isotopic composition of the fragments. An outline drawing of the telescope is shown in Fig. 1. The telescope basically consists of three separate

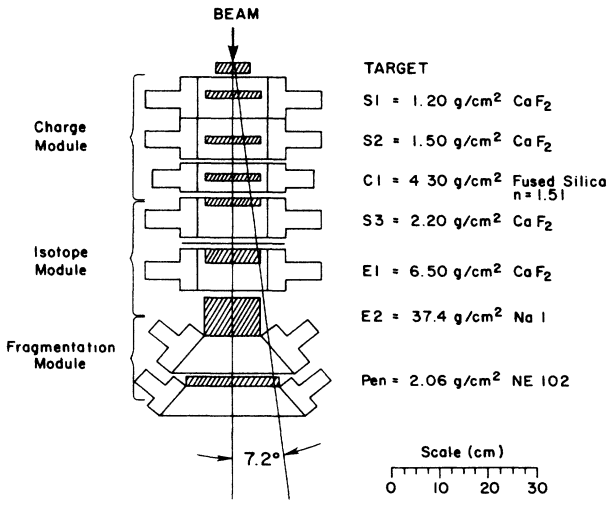

FIG. 1. Schematic representation of the charge and isotope telescope used in these studies.

modules, a charge identification module, an isotope identification module, and a fragment module. For the study in this paper the isotope identification module was used in addition to the fragment module.

As noted in paper I, for the CH_2 and C targets, the half angle of the acceptance cone for the bottom counter of the charge module is 7.7°. As the particle penetrates further into the total energy counters in the isotope identification module this half-angle decreases to 6.6° at $E1$ and 5.6° at $E2$. However, for the penetration counter this angle is 7.4°, thus virtually all particles within the acceptance of the charge module should also be seen in this counter. As also noted in paper I, for the worst possible case at which isotopic analysis is carried out, a B fragment at $\sim$500 MeV/nucleon; assuming a transverse momentum distribution with a $\sigma \sim 175$ MeV/nucleon[5,6] leads to a $\pm 3\sigma$ scattering angle $\sim 4.4°$ or less than the half angle at $E2$. Furthermore, it is observed that all principal fragments identified in the charge module are accompanied by events identified also as the principal fragment in the $E1$ and $E2$ counters, thus there is essentially no loss of events between the charge module and the isotope module due to a large scatter or a miss of the E counters.

No evidence of multiple particle events or particle pile up that might also affect the isotopic resolution has ever been detected at the low rates $\lesssim 3000$ events per dump used in these studies. Particle pile up effects could first be observed when the beam intensity exceeded $\sim 15\,000$ events per dump.

In this method of analysis the individual isotopes are identified by the Cerenkov x total energy technique, which requires the particles to stop in the thick total energy counters. The fragment identification scintillation counters are used to determine that the principal fragment has indeed stopped in the last total energy counter and also to identify the charge of the lower Z fragments that penetrate to this counter. The Cerenkov x total energy technique was first employed by our group using a specifically designed large area telescope flown on balloons to study the isotopic composition of cosmic rays (Webber *et al.*[7]). In these balloon experiments a mass resolution $\lesssim 0.3$ u was achieved for nuclei of several hundred MeV/nucleon with Z between 6–20. The telescope built for the Bevalac studies is a smaller-higher resolution version of the instrument flown on balloons. The analysis techniques used for the Bevalac studies have been adapted and refined from those used for the balloon borne instruments.[8,9]

In this method of analysis the first step is to identify separately the charge of each particle, as has been done in the charge module. Then a two-dimensional matrix of events is made for each charge, consisting of the Cerenkov output versus the total energy lost in the stopping counter, the result of which is shown in Fig. 2. In this representation the isotopes of each charge are found to lie along roughly parallel lines, with the different energies incident on the telescope spread out along the "mass" lines. For a monoenergetic incident energy distribution each isotope should form a separate clump in $C \times E$ space, however, because of interactions occurring throughout the target, the different secondary isotopes that are produced are spread out more or less uniformly along the mass lines over an energy range of $\sim$10–50 MeV/nucleon depending on the thickness of the target and the beam charge. The separation of the mass lines in u depends on the resolution of the Cerenkov and total energy counters.[8,9] Generally, the resolution in the Cerenkov counter, which depends mainly on photoelectron statistics, is the dominant contributor to the overall mass resolution. In our experiment the mass resolution for this counter is found to be ~ 0.12 u for the lower Z fragments increasing to ~ 0.23 u for the higher Z fragments from ^{56}Fe beams (see Table I). In order to measure the mass distribution of fragments from a particular beam nucleus it is necessary to "tune" the index of refraction of the Cerenkov counter and the total thickness of the energy counters, since the technique is most sensitive in an energy range $\sim$100–450 MeV/nucleon wide just above the Cerenkov threshold. Generally, the highest specific output in photoelectrons was obtained with Cerenkov counters of index of refraction, n between 1.26–1.51, corresponding to thresholds $\sim$320–600 MeV/nucleon. Thus, depending on the beam charge, the isotopic composition could be measured in the energy range from $\sim$450 MeV/nucleon to $\sim$1 GeV/nucleon. In Table I we list the subset of 24 out of the 42 total beam runs in which the isotopic composition was measured (see Table I in paper I for a complete list of the runs). Also shown in Table I is the index of refraction of the Cerenkov counter used, the charge range over which mass analysis was achieved, and the mass resolution σ in u.

In Fig. 2(a)–(c) we show three sample matrices—Cerenkov versus total energy for (1) N isotopes from ^{16}O fragmentation, (2) Al isotopes from ^{28}Si fragmentation, and (3) Mn isotopes from ^{56}Fe fragmentation. These matrices are obtained subject to the consistency criteria described in the following section. These matrices form the basic data from which the mass distributions for each fragment charge are obtained.

The next step in this procedure is to construct mass histograms from these matrices by summing events parallel to the mass lines. Mass histograms for the three sample matrices are shown in Figures 3(a)–(c). Conversion of these mass histograms to mass fractions and ultimately to isotopic cross sections will be discussed in the following section. Here we should note that use is made of the fragment counters to identify the lower Z fragments that accompany the principal fragments. These lower Z fragments penetrate to the fragment counters and may be separately identified in them. As the difference between the beam and fragment charge becomes greater, these lower Z fragments make an increasingly important contribution to the pulse heights measured in both the Cerenkov and stopping E counter. Because of the many channels possible for these lower Z fragments they are the principal contributor to a slow degradation in mass resolution as the beam-principal fragment charge difference increases. Whenever this lower Z fragment contribution becomes $\sim$10% or larger of that of the principal fragment, a correction to the pulse height in the C and E counters is made based on the identified charge of

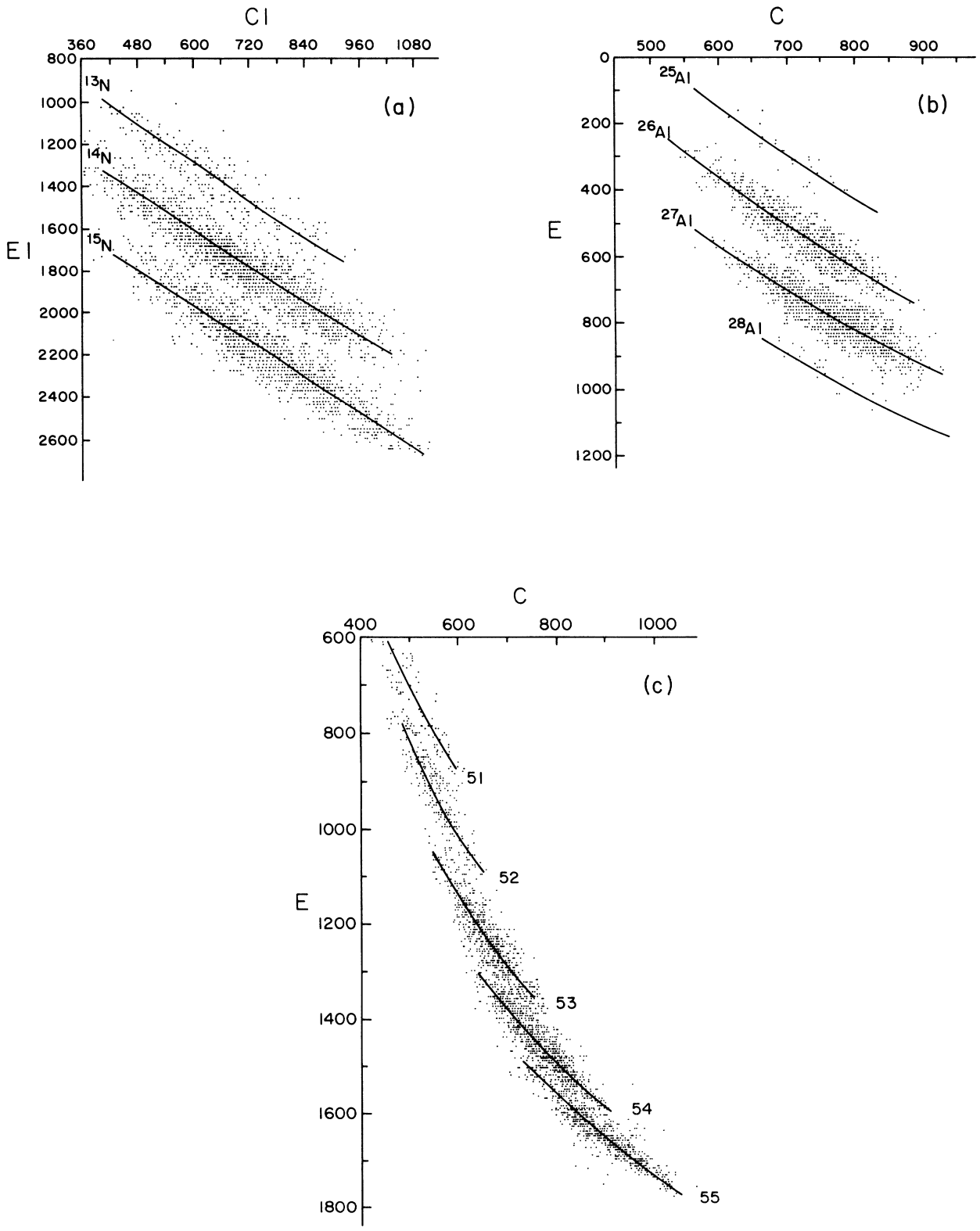

FIG. 2. (a) Cross plot of Cerenkov versus total energy for N isotopes from ^{16}O fragmentation in a CH_2 target. (b) Same as (a) except for Al isotopes from ^{28}Si fragmentation in a CH_2 target. (c) Same as (a) except for Mn isotopes from ^{56}Fe fragmentation in a C target.

TABLE I. Isotopic fragmentation runs.

Charge	Beam energy (MeV/nucleon)	Target energy (MeV/nucleon)	Cerenkov counter n	Mass analysis charge range Z	Mass resolution σ (u)
B	550	486	1.405	4	0.12
^{12}C	450	410	1.505	4–6	0.10
^{12}C	610	561	1.355	4–6	0.12
^{14}N	550	516	1.405	4–7	0.11
^{16}O	500	440	1.515	5–8	0.14
^{16}O	640	591	1.355	6–8	0.13
^{20}Ne	540	468	1.515	6–10	0.15
^{20}Ne	645	599	1.338	8–10	0.14
Na	640	461	1.405	10	0.15
^{24}Mg	540	481	1.505	7–12	0.14
^{24}Mg	790	739	1.263	8–12	0.15
^{27}Al	640	582	1.405	10–13	0.14
^{28}Si	830	770	1.263	10–14	0.15
^{32}S	720	649	1.338	10–16	0.15
^{40}Ar	590	521	1.505	12–18	0.15
^{40}Ar	870	792	1.263	14–18	0.15
^{40}Ca	760	672	1.338	14–20	0.16
^{56}Fe	580	520	1.505	24–26	0.21
^{56}Fe	600	521	1.505	17–26	0.20
^{56}Fe	710	662	1.515	17–26	0.27
^{56}Fe	810	724	1.355	16–26	0.23
^{56}Fe	1010	944	1.355	18–26	0.29
^{56}Fe	1180	1089	1.263	24–26	0.21
^{58}Ni	640	571	1.505	26–28	0.22

the low Z fragment in the penetrating counters. For example, if this charge is identified as $Z=6$ a pulse height corresponding to this charge is subtracted from the pulse height measured in the Cerenkov and stopping E counter. Using this procedure we are able to achieve a nearly constant mass resolution throughout the principal fragment charge range down to a charge at which this fragment penetrates the total energy counters. This determines the lower charge limit for which the isotopes can be measured as indicated in Table I.

III. DATA ANALYSIS AND THE DETERMINATION OF THE ISOTOPE CROSS SECTIONS

As described earlier, in order to apply the Cerenkov x total energy technique, it is first necessary to identify and separately isolate each fragment charge. This has already been achieved in order to determine the charge changing cross sections presented in paper II. However, the particles we wish to isotopically analyze penetrate further into the telescope and have additional nuclear interactions. To remove these interactions, additional tighter consistency criteria corresponding to $\pm 2.5\sigma$, where σ is the resolution of each counter, are placed on the expected outputs of *all* of the combinations of counters in the telescope including $S1$–$S3$ and C and $E1$ but not including the stopping total energy counter. These criteria must be applied very carefully, particularly to C and $E1$ to assure that isotopes in the wings of the distributions for these counters are not removed. The boundaries of these criteria are changed and the resulting mass histograms examined to study this effect. We believe that any mass dependent bias introduced by this procedure is negligible except possibly for isotopes far from the mass centroid, whose cross sections are small and unimportant for this study.

The matrices shown in Figures 2(a)–2(c) and the histograms shown in Figs. 3(a)–3(c) have these criteria applied. Generally, these criteria reduce the number for events of a given charge available for mass analysis by ~ 20–50% from the number used to determine the charge changing cross sections. This fraction depends on the fragment charge and energy and the thickness of the total energy counters. This decrease is consistent with the fractional number of interactions to be expected in the various counters as the fragment comes to rest.

To obtain a set of mass fractions from this data that directly correspond to the charge abundances derived in paper II we must make several corrections to the raw abundances obtained from the mass histograms. The two most significant ones are (1) a correction to the top of the total energy counters for interactions occurring in these counters. This is a straightforward correction given by

$$N_{\rm obs}(A)=N_{\rm CM}(A)\exp^{-X_A/\lambda_A(A)},$$

where $N_{\rm obs}(A)$ is the observed number of events of fragment mass A after the mass selection criteria, $N_{\rm CM}(A)$ is the number emerging from the charge module, and X_A is the average thickness traversed in the total energy counters before fragment mass A stops and $\lambda_A(A)$ is the interaction mean free path of each fragment mass in the total energy counter. The interaction mean free paths are obtained from

$$\lambda_A(A)=\frac{m}{\sigma_A},$$

where

$$\sigma_A=\pi r_0^2(A_t^{1/3}+A_B^{1/3}-b)^2,$$

where $r_0=1.35\times10^{-13}$ cm and b, the overlap parameter, is adapted from our study of the total interaction cross sections, reported in paper I. This correction, which can be made with good accuracy, changes the relative raw mass abundance fractions by ~ 10–$20\,\%$ at most for each charge. These corrected mass fractions are then normal-

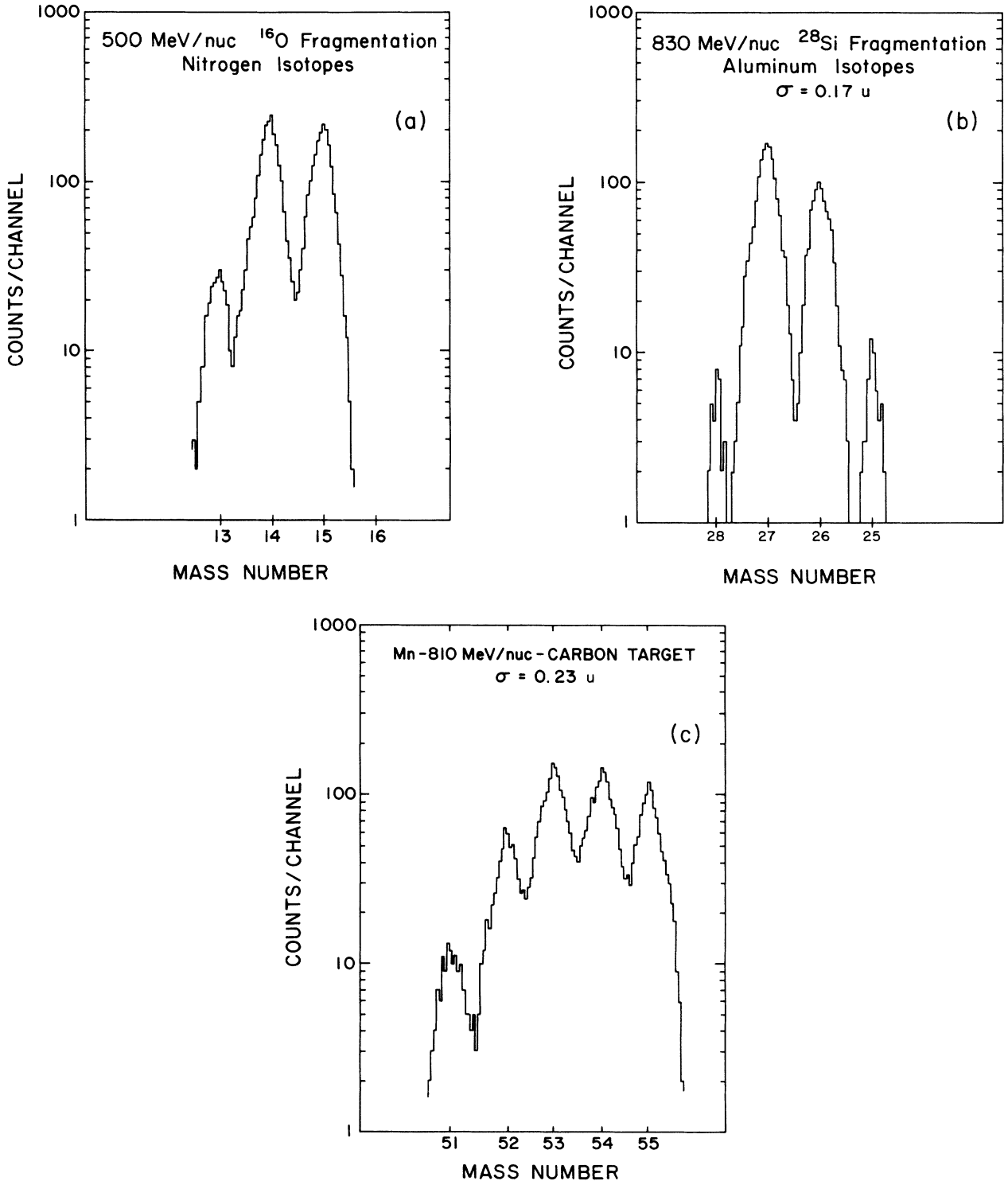

FIG. 3. (a) Mass histogram for N isotopes from ^{16}O fragmentation in a CH_2 target. (b) Mass histogram for Al isotopes from ^{28}Si fragmentation in a CH_2 target. (c) Mass histogram for Mn isotopes from ^{56}Fe fragmentation in a C target.

ized to one for each charge giving what we define as the mass yield distribution. These mass yield distributions are then corrected to the top of the telescope using an interaction connection similar to the aforementioned but in the charge telescope. The ratios at the top of the telescope would be the ratios of the isotopic cross sections of a given charge for an infinitely thin target. However, since our targets are thick some of the fragments produced will have secondary interactions before they leave the target. In order to correct for these secondary interactions and derive a set of isotopic cross sections for the incident beam charge we use a one-dimensional diffusion equation of the form

$$\frac{dN_{Af}(x)}{dx} = \frac{-\sigma_{Af} N_{Af}(x)}{m_{\text{tar}}} + \sum_{A_i > A_f} \frac{\sigma_{A_i A_f}}{m_{\text{tar}}} - N_{Ai}(x) .$$

This equation is completely analogous to that used to derive the charge changing cross sections, σ_{Zf}, in paper II. Here N_{Af} is the abundance of a fragment with mass A_f measured at the bottom of the target, σ_{Af} is the total mass changing cross section for this isotope, $\sigma_{A_i A_f}$ is the partial cross section from charge Z_i, mass A_i (including the beam charge), into charge Z_f, A_f, and N_{Ai} is the abundance of this heavier isotope. In this equation it is assumed that energy loss in the target is not important and the derived cross sections are appropriate to the average energy in the target. In this program the charge fraction of each fragment charge relative to the beam charge as obtained in paper II, and the isotopic fractions normalized to one for each charge, are inputs to the program which then calculates the appropriate isotopic cross section to fragment A_f from the beam nucleus A_B. This program requires estimates of all the relevant secondary mass changing cross sections as well. The initial estimates of these secondary cross sections were based on the Tsao and Silberberg,[10] semiempirical formula. As more cross sections became available from our study, it was possible to develop a new semiempirical formula [Webber,[11] also presented in paper IV (Ref. 12)]. This formula was used to determine the secondary/primary cross sections in an iterative self-consistent way and these were used for all of the secondary mass changing cross sections. The primary isotopic cross sections from various beam nuclei we derive in this way are shown for carbon and hydrogen targets in Table II. The data for helium targets are shown in Table III. We have noted earlier that most of these isotopic cross sections are measured at a very similar energy, $\sim 600 \pm 200$ MeV/nucleon, for each beam charge. No significant energy dependence of the mass fractions is observed over this energy range, therefore the cross sections listed in Tables II or III represent averages of the appropriate run energies as given in Table I. For some beam charges where the isotopic cross sections are measured over a wider band of energies, e.g., ^{12}C, ^{16}O, ^{40}Ar, and ^{56}Fe, the possible energy dependence of the mass fractions is discussed in a later section.

TABLE II. Isotopic cross-sections in carbon and hydrogen targets measured at 600 MeV/nucleon (Ref. 10). U.N.H. denotes the University of New Hampshire hydrogen calculation (Ref. 12). T&S denotes Tsao and Silberberg's hydrogen calculations. Errors: $A = \pm 1.5\%$, $B = \pm 3\%$, $C = \pm 5\%$, and $D = \pm 10\%$.

From Z, A	To Z, A	Carbon isotopic cross section (error)	Hydrogen charge cross section	Hydrogen mass fraction	Hydrogen isotopic cross section (error)	U.N.H. hydrogen calculations	T&S hydrogen calculations
5,11	4,10	10.2 (*B*)	36.6	0.137	5.0 (*B*)	7.1	6.1
5,11	4,9	14.4 (*B*)	36.6	0.178	6.5 (*B*)	13.2	9.3
5,11	4,7	46.2 (*A*)	36.6	0.686	25.1 (*A*)	15.8	9.6
6,12	6,11	53.6 (*A*)	29.7	0.966	28.7 (*B*)	28.6	28.8
6,12	6,10	2.1 (*C*)	29.7	0.037	1.1 (*D*)	2.0	3.3
6,12	5,11	70.7 (*A*)	49.8	0.657	32.7 (*A*)	35.4	27.8
6,12	5,10	38.6 (*A*)	49.8	0.343	17.1 (*A*)	14.2	23.6
6,12	4,10	5.6 (*C*)	13.9	0.180	2.5 (*C*)	1.8	2.9
6,12	4,9	9.6 (*B*)	13.9	0.309	4.3 (*B*)	4.8	5.3
6,12	4,7	15.5 (*B*)	13.9	0.511	7.1 (*B*)	7.9	11.1
7,14	7,13	13.3 (*B*)	8.6	0.872	7.5 (*B*)	9.4	11.4
7,14	7,12	2.0 (*D*)	8.6	0.128	1.1 (*D*)	1.8	2.2
7,14	6,13	21.3 (*A*)	74.3	0.129	9.6 (*A*)	10.5	12.9
7,14	6,12	117.2 (*A*)	74.3	0.701	52.1 (*A*)	40.1	46.7
7,14	6,11	27.5 (*A*)	74.3	0.157	11.7 (*B*)	10.3	13.4
7,14	6,10	2.1 (*D*)	74.3	0.012	0.9 (*D*)	0.5	2.7
7,14	5,11	39.8 (*A*)	27.4	0.639	17.5 (*A*)	13.4	17.7
7,14	5,10	23.9 (*A*)	27.4	0.361	9.9 (*A*)	9.2	19.6
7,14	4,10	3.5 (*D*)	13.7	0.117	1.6 (*D*)	1.8	1.6
7,14	4,9	4.1 (*D*)	13.7	0.146	2.0 (*D*)	3.9	4.5
7,14	4,7	21.6 (*B*)	13.7	0.737	10.1 (*B*)	8.1	9.4

TABLE II. (*Continued*).

From Z, A	To Z, A	Carbon isotopic cross section (error)	Hydrogen charge cross section	Hydrogen mass fraction	Hydrogen isotopic cross section (error)	U.N.H. hydrogen calculations	T&S hydrogen calculations
8,16	8,15	84.0 (*A*)	31.5	0.962	30.3 (*A*)	30.8	29.8
8,16	8,14	2.6 (*D*)	31.5	0.038	1.2 (*D*)	2.0	2.9
8,16	7,15	73.2 (*A*)	71.9	0.485	34.9 (*A*)	36.1	38.6
8,16	7,14	66.8 (*A*)	71.9	0.431	31.0 (*A*)	32.6	32.8
8,16	7,13	12.6 (*B*)	71.9	0.079	5.7 (*C*)	5.7	3.9
8,16	7,12	0.6 (*D*)	71.9	0.004	0.3 (*D*)	0.2	1.8
8,16	6,14	3.3 (*C*)	66.8	0.025	1.7 (*C*)	1.8	2.1
8,16	6,13	41.0 (*A*)	66.8	0.269	18.0 (*A*)	18.7	16.3
8,16	6,12	79.2 (*A*)	66.8	0.503	33.6 (*A*)	39.5	38.7
8,16	6,11	26.5 (*A*)	66.8	0.178	11.9 (*B*)	10.1	16.0
8,16	6,10	3.2 (*D*)	66.8	0.024	1.6 (*D*)	0.3	2.3
8,16	5,12	2.4 (*D*)	26.2	0.042	1.1 (*D*)	1.5	2.0
8,16	5,11	36.0 (*A*)	26.2	0.595	15.6 (*B*)	16.7	14.8
8,16	5,10	24.8 (*A*)	26.2	0.366	9.6 (*B*)	11.3	9.1
10,20	10,19	65.6 (*A*)	29.3	0.956	28.0 (*A*)	32.6	18.5
10,20	10,18	2.2 (*D*)	29.3	0.044	1.3 (*D*)	2.0	2.4
10,20	9,19	52.4 (*A*)	48.3	0.532	25.7 (*D*)	26.4	25.8
10,20	9,18	39.6 (*A*)	48.3	0.393	19.0 (*A*)	23.5	18.5
10,20	9,17	7.2 (*C*)	48.3	0.068	3.3 (*C*)	3.5	9.3
10,20	9,16	1.0 (*D*)	48.3	0.006	0.3 (*D*)	0.2	1.6
10,20	8,18	7.2 (*B*)	74.6	0.043	3.2 (*C*)	3.8	4.5
10,20	8,17	26.6 (*A*)	74.6	0.164	12.2 (*B*)	19.4	18.0
10,20	8,16	95.2 (*A*)	74.6	0.563	42.0 (*A*)	43.2	32.0
10,20	8,15	35.8 (*A*)	74.6	0.217	16.2 (*B*)	14.3	12.4
10,20	8,14	2.7 (*D*)	74.6	0.013	1.0 (*D*)	0.9	2.0
10,20	7,16	2.6 (*D*)	61.8	0.019	1.2 (*D*)	2.1	3.2
10,20	7,15	63.5 (*A*)	61.8	0.450	27.8 (*A*)	23.4	11.0
10,20	7,14	65.7 (*A*)	61.8	0.456	28.2 (*A*)	27.8	12.2
10,20	7,13	11.0 (*B*)	61.8	0.066	4.1 (*C*)	3.6	2.7
10,20	7,12	1.3 (*D*)	61.8	0.006	0.4 (*D*)	0.3	1.3
10,20	6,14	6.4 (*C*)	59.2	0.039	2.3 (*C*)	0.9	3.4
10,20	6,13	36.2 (*A*)	59.2	0.265	15.7 (*A*)	13.8	11.0
10,20	6,12	81.3 (*A*)	59.2	0.584	34.6 (*A*)	33.7	14.4
10,20	6,11	17.5 (*B*)	59.2	0.106	6.3 (*C*)	7.3	7.5
10,20	6,10	0.8 (*D*)	59.2	0.005	0.3 (*D*)	0.2	1.6
11,23	10,23	13.7 (*B*)	80.3	0.105	8.4 (*B*)	5.8	6.4
11,23	10,22	39.2 (*A*)	80.3	0.298	23.9 (*A*)	16.5	18.5
11,23	10,21	48.5 (*A*)	80.3	0.365	29.3 (*A*)	29.8	23.0
11,23	10,20	25.4 (*A*)	80.3	0.189	15.2 (*B*)	18.9	18.8
11,23	10,19	6.0 (*C*)	80.3	0.044	3.5 (*C*)	2.7	3.9
12,24	12,23	88.6 (*A*)	34.3	0.910	31.2 (*A*)	33.8	31.9
12,24	12,22	7.8 (*C*)	34.3	0.090	3.1 (*C*)	2.0	1.8
12,24	11,23	69.2 (*A*)	84.2	0.523	44.0 (*A*)	45.5	25.8
12,24	11,22	59.8 (*A*)	84.2	0.435	36.6 (*A*)	34.7	22.4
12,24	11,21	6.6 (*C*)	84.2	0.043	3.6 (*C*)	4.7	8.2
12,24	10,22	19.4 (*B*)	63.4	0.185	11.7 (*B*)	9.0	8.7
12,24	10,21	39.0 (*A*)	63.4	0.368	23.3 (*A*)	26.2	17.4
12,24	10,20	39.2 (*A*)	63.4	0.369	23.4 (*A*)	27.7	21.7
12,24	10,19	7.2 (*C*)	63.4	0.065	4.1 (*C*)	5.5	5.6
12,24	10,18	1.6 (*D*)	63.4	0.014	0.9 (*D*)	0.3	1.6
12,24	9,21	1.2 (*D*)	28.9	0.014	0.4 (*D*)	0.1	0.5
12,24	9,20	5.8 (*C*)	28.9	0.107	3.1 (*C*)	2.6	4.1
12,24	9,19	18.7 (*A*)	28.9	0.360	10.4 (*B*)	13.7	12.6
12,24	9,18	21.5 (*A*)	28.9	0.419	12.1 (*B*)	12.4	12.5
12,24	9,17	4.8 (*C*)	28.9	0.090	2.6 (*C*)	2.0	6.4

TABLE II. (*Continued*).

From Z, A	To Z, A	Carbon isotopic cross section (error)	Hydrogen charge cross section	Hydrogen mass fraction	Hydrogen isotopic cross section (error)	U.N.H. hydrogen calculations	T&S hydrogen calculations
12,24	8,18	6.1 (*C*)	58.8	0.056	3.3 (*C*)	2.0	4.2
12,24	8,17	23.6 (*A*)	58.8	0.214	12.6 (*B*)	13.5	12.7
12,24	8,16	60.7 (*A*)	58.8	0.558	32.8 (*A*)	30.4	14.8
12,24	8,15	16.6 (*B*)	58.8	0.146	8.6 (*B*)	9.9	9.8
12,24	8,14	2.8 (*D*)	58.8	0.026	1.5 (*D*)	0.6	1.3
12,24	7,16	4.3 (*D*)	36.0	0.047	1.7 (*D*)	1.3	2.2
12,24	7,15	32.9 (*A*)	36.0	0.389	14.0 (*B*)	13.7	7.6
12,24	7,14	30.0 (*A*)	36.0	0.350	12.6 (*B*)	16.5	8.4
12,24	7,13	13.4 (*B*)	36.0	0.167	6.0 (*C*)	3.3	1.8
12,24	7,12	3.3 (*D*)	36.0	0.047	1.7 (*D*)	0.4	0.4
13,27	13,26	63.7 (*A*)	38.1	0.953	36.3 (*A*)	37.9	32.7
13,27	13,25	4.2 (*C*)	38.1	0.047	1.8 (*D*)	11.5	4.1
13,27	12,26	63.7 (*A*)	112.6	0.356	40.1 (*A*)	34.1	25.7
13,27	12,25	69.2 (*A*)	112.6	0.378	42.6 (*A*)	45.3	29.3
13,27	12,24	45.1 (*A*)	112.6	0.242	27.2 (*A*)	28.1	19.0
13,27	11,23	3.6 (*D*)	112.6	0.024	2.7 (*C*)	4.7	5.2
13,27	11,25	5.4 (*C*)	51.5	0.050	2.6 (*C*)	2.7	3.6
13,27	11,24	21.1 (*A*)	51.5	0.221	11.4 (*B*)	12.5	9.4
13,27	11,23	46.1 (*A*)	51.5	0.493	25.4 (*A*)	24.4	18.1
13,27	11,22	17.2 (*B*)	51.5	0.186	9.6 (*B*)	10.5	14.0
13,27	11,21	2.6 (*D*)	51.5	0.027	1.4 (*D*)	1.0	2.7
13,27	10,24	1.3 (*D*)	49.6	0.010	0.5 (*D*)	0.1	0.4
13,27	10,23	9.0 (*C*)	49.6	0.113	5.6 (*C*)	0.4	2.1
13,27	10,22	25.5 (*A*)	49.6	0.300	14.9 (*A*)	7.8	9.5
13,27	10,21	29.5 (*A*)	49.6	0.327	16.2 (*A*)	26.5	15.1
13,27	10,20	20.3 (*B*)	49.6	0.220	10.9 (*B*)	18.1	14.4
13,27	10,19	3.1 (*D*)	49.6	0.030	1.5 (*D*)	2.3	2.9
14,28	14,27	92.0 (*A*)	32.6	0.957	31.2 (*A*)	34.0	32.6
14,28	14,26	3.0 (*D*)	32.6	0.043	1.4 (*D*)	1.8	1.2
14,28	13,27	95.0 (*A*)	83.8	0.618	51.8 (*A*)	46.6	26.4
14,28	13,26	58.5 (*A*)	83.8	0.362	30.3 (*A*)	32.5	17.0
14,28	13,25	4.0 (*C*)	83.8	0.021	1.8 (*D*)	3.9	6.9
14,28	12,26	32.9 (*A*)	80.8	0.197	15.9 (*A*)	14.0	16.1
14,28	12,25	56.2 (*A*)	80.8	0.337	27.2 (*A*)	34.6	23.1
14,28	12,24	66.1 (*A*)	80.8	0.408	33.0 (*A*)	35.2	20.8
14,28	12,23	6.9 (*C*)	80.8	0.057	4.6 (*C*)	8.7	7.9
14,28	11,25	1.2 (*D*)	37.5	0.021	0.8 (*D*)	0.5	0.5
14,28	11,24	9.5 (*B*)	37.5	0.136	5.1 (*C*)	7.7	5.4
14,28	11,23	31.1 (*A*)	37.5	0.504	18.9 (*A*)	21.8	14.1
14,28	11,22	20.2 (*A*)	37.5	0.304	11.4 (*B*)	14.7	14.7
14,28	11,21	2.3 (*D*)	37.5	0.032	1.2 (*D*)	1.9	5.6
14,28	10,23	1.0 (*D*)	37.1	0.013	0.5 (*D*)	0.3	0.9
14,28	10,22	13.2 (*B*)	37.1	0.210	7.8 (*B*)	3.7	5.6
14,28	10,21	21.3 (*A*)	37.1	0.332	12.3 (*A*)	14.4	11.8
14,28	10,20	21.8 (*A*)	37.1	0.358	13.3 (*A*)	15.0	14.9
14,28	10,19	5.3 (*C*)	37.1	0.081	3.0 (*C*)	3.9	3.8
16,32	16,31	92.1 (*A*)	34.9	0.948	33.1 (*A*)	33.6	33.7
16,32	16,30	3.1 (*D*)	34.9	0.052	1.8 (*D*)	1.8	0.8
16,32	15,31	65.5 (*A*)	79.6	0.523	41.6 (*A*)	59.6	26.4
16,32	15,30	52.6 (*A*)	79.6	0.413	32.9 (*A*)	34.4	15.4
16,32	15,29	8.0 (*C*)	79.6	0.058	4.6 (*C*)	4.0	5.1
16,32	15,28	1.0 (*D*)	79.6	0.006	0.5 (*D*)	0.2	0.6
16,32	14,30	22.4 (*A*)	104.8	0.149	15.6 (*A*)	18.8	28.8
16,32	14,29	50.6 (*A*)	104.8	0.335	35.1 (*A*)	48.9	25.7
16,32	14,28	63.4 (*A*)	104.8	0.422	44.2 (*A*)	42.0	19.4

TABLE II. (*Continued*).

From Z, A	To Z, A	Carbon isotopic cross section (error)	Hydrogen charge cross section	Hydrogen mass fraction	Hydrogen isotopic cross section (error)	U.N.H. hydrogen calculations	T&S hydrogen calculations
16,32	14,27	13.3 (*B*)	104.8	0.086	9.0 (*B*)	10.2	6.3
16,32	14,26	1.5 (*D*)	104.8	0.009	0.9 (*D*)	0.4	0.9
16,32	13,29	2.2 (*D*)	52.3	0.019	1.0 (*D*)	1.3	0.5
16,32	13,28	14.2 (*B*)	52.3	0.161	8.4 (*B*)	11.6	7.3
16,32	13,27	41.3 (*A*)	52.3	0.482	25.2 (*A*)	27.0	15.9
16,32	13,26	24.5 (*A*)	52.3	0.279	14.6 (*B*)	16.4	17.7
16,32	13,25	4.9 (*C*)	52.3	0.050	2.6 (*C*)	2.7	4.6
16,32	13,24	1.0 (*D*)	52.3	0.010	0.5 (*D*)	0.2	0.6
16,32	12,27	1.8 (*D*)	69.2	0.014	1.0 (*D*)	0.4	1.5
16,32	12,26	17.3 (*B*)	69.2	0.171	11.8 (*B*)	6.0	7.5
16,32	12,25	36.8 (*A*)	69.2	0.340	23.5 (*A*)	24.9	15.9
16,32	12,24	40.7 (*A*)	69.2	0.395	27.3 (*A*)	26.4	14.3
16,32	12,23	8.2 (*C*)	69.2	0.074	5.1 (*C*)	6.3	5.4
16,32	12,22	0.8 (*D*)	69.2	0.007	0.5 (*D*)	0.5	1.2
16,32	11,24	6.4 (*D*)	33.5	0.099	3.3 (*C*)	4.8	3.7
16,32	11,23	29.1 (*A*)	33.5	0.516	17.3 (*A*)	16.3	9.7
16,32	11,22	19.0 (*B*)	33.5	0.340	11.4 (*B*)	11.5	10.1
16,32	11,21	2.7 (*D*)	33.5	0.045	1.5 (*D*)	1.8	3.9
16,32	10,22	10.1 (*B*)	31.5	0.168	5.3 (*C*)	2.5	2.8
16,32	10,21	21.2 (*A*)	31.5	0.333	10.5 (*B*)	13.6	8.0
16,32	10,20	22.7 (*A*)	31.5	0.381	12.0 (*B*)	13.5	10.1
16,32	10,19	4.4 (*C*)	31.5	0.076	2.4 (*C*)	2.7	2.6
16,32	10,18	1.5 (*D*)	31.5	0.025	0.8 (*D*)	0.3	0.8
18,40	18,39	146.4 (*A*)	95.1	0.632	60.1 (*A*)	60.8	46.2
18,40	18,38	72.3 (*A*)	95.1	0.306	29.1 (*A*)	29.4	15.6
18,40	18,37	8.4 (*C*)	95.1	0.062	5.9 (*C*)	4.2	2.0
18,40	17,39	39.1 (*A*)	132.2	0.218	28.8 (*A*)	42.9	18.5
18,40	17,38	34.9 (*A*)	132.2	0.190	25.1 (*A*)	25.3	20.4
18,40	17,37	59.3 (*A*)	132.2	0.327	43.2 (*A*)	43.1	22.4
18,40	17,36	38.0 (*A*)	132.2	0.199	26.3 (*A*)	25.0	20.6
18,40	17,35	12.3 (*C*)	132.2	0.067	8.8 (*B*)	5.0	9.7
18,40	16,38	0.8 (*D*)	98.2	0.004	0.4 (*D*)	1.9	0.3
18,40	16,37	5.1 (*C*)	98.2	0.040	3.9 (*C*)	1.0	1.5
18,40	16,36	19.3 (*B*)	98.2	0.155	15.2 (*A*)	10.6	10.1
18,40	16,35	32.6 (*A*)	98.2	0.265	26.0 (*A*)	32.4	16.6
18,40	16,34	51.0 (*A*)	98.2	0.416	40.9 (*A*)	39.5	24.1
18,40	16,33	15.3 (*B*)	98.2	0.114	11.2 (*B*)	13.7	8.3
18,40	16,32	1.1 (*D*)	98.2	0.006	0.6 (*D*)	1.6	2.5
18,40	15,35	1.2 (*D*)	70.3	0.010	0.7 (*D*)	0.3	0.4
18,40	15,34	6.3 (*C*)	70.3	0.070	4.9 (*C*)	4.0	2.4
18,40	15,33	23.8 (*A*)	70.3	0.269	18.9 (*A*)	17.3	11.9
18,40	15,32	35.9 (*A*)	70.3	0.400	28.1 (*A*)	25.7	12.6
18,40	15,31	24.0 (*A*)	70.3	0.250	17.6 (*A*)	11.7	8.4
18,40	15,30	2.2 (*D*)	70.3	0.011	0.8 (*D*)	1.7	1.8
18,40	14,32	4.1 (*C*)	75.3	0.045	3.4 (*C*)	1.9	3.1
18,40	14,31	17.6 (*B*)	75.3	0.187	14.1 (*A*)	14.3	10.3
18,40	14,30	40.1 (*A*)	75.3	0.422	31.8 (*A*)	31.7	15.2
18,40	14,29	27.6 (*A*)	75.3	0.278	20.9 (*A*)	20.1	9.8
18,40	14,28	9.2 (*C*)	75.3	0.068	5.1 (*C*)	3.7	3.0
18,40	13,30	1.2 (*D*)	46.1	0.013	0.6 (*D*)	0.3	1.1
18,40	13,29	11.8 (*B*)	46.1	0.176	8.1 (*B*)	4.0	6.1
18,40	13,28	20.5 (*A*)	46.1	0.299	13.8 (*B*)	12.9	10.6
18,40	13,27	33.1 (*A*)	46.1	0.464	21.4 (*A*)	11.1	8.1
18,40	13,26	4.2 (*D*)	46.1	0.048	2.2 (*D*)	2.6	3.0
18,40	12,27	4.1 (*C*)	38.7	0.059	2.3 (*D*)	2.8	3.7
18,40	12,26	23.0 (*A*)	38.7	0.390	15.1 (*B*)	12.5	7.4

TABLE II. (*Continued*).

From Z, A	To Z, A	Carbon isotopic cross section (error)	Hydrogen charge cross section	Hydrogen mass fraction	Hydrogen isotopic cross section (error)	U.N.H. hydrogen calculations	T&S hydrogen calculations
18,40	12,25	23.1 (*A*)	38.7	0.367	14.2 (*B*)	13.5	6.6
18,40	12,24	12.7 (*B*)	38.7	0.173	6.7 (*C*)	2.8	2.7
18,40	12,23	1.0 (*D*)	38.7	0.010	0.4 (*D*)	0.2	0.5
20,40	20,39	92.1 (*A*)	31.8	0.937	29.8 (*A*)	26.7	19.6
20,40	20,38	4.6 (*D*)	31.8	0.063	2.0 (*D*)	1.8	0.4
20,40	19,39	58.8 (*A*)	66.7	0.580	38.7 (*A*)	47.0	44.6
20,40	19,38	38.5 (*A*)	66.7	0.373	24.9 (*A*)	24.8	32.4
20,40	19,37	4.1 (*C*)	66.7	0.033	2.2 (*D*)	1.0	27.0
20,40	19,36	1.5 (*D*)	66.7	0.013	0.9 (*D*)	0.1	0.3
20,40	18,38	31.9 (*A*)	94.1	0.235	22.1 (*A*)	28.8	23.7
20,40	18,37	62.8 (*A*)	94.1	0.447	42.1 (*A*)	44.0	34.9
20,40	18,36	39.2 (*A*)	94.1	0.275	25.9 (*A*)	22.3	20.2
20,40	18,35	6.2 (*C*)	94.1	0.043	4.0 (*C*)	3.9	3.1
20,40	17,37	4.0 (*C*)	55.8	0.057	3.2 (*C*)	4.1	6.0
20,40	17,36	18.1 (*B*)	55.8	0.222	12.4 (*B*)	17.2	18.5
20,40	17,35	36.4 (*A*)	55.8	0.471	26.3 (*A*)	24.5	30.6
20,40	17,34	17.5 (*B*)	55.8	0.219	12.2 (*B*)	12.0	12.0
20,40	17,33	2.4 (*D*)	55.8	0.030	1.7 (*D*)	2.0	3.4
20,40	16,36	1.3 (*D*)	78.3	0.013	1.0 (*D*)	0.3	0.7
20,40	16,35	5.6 (*C*)	78.3	0.043	3.4 (*C*)	3.3	4.1
20,40	16,34	31.6 (*A*)	78.3	0.271	21.2 (*A*)	16.8	18.4
20,40	16,33	46.0 (*A*)	78.3	0.407	31.9 (*A*)	28.0	21.6
20,40	16,32	24.5 (*A*)	78.3	0.222	17.4 (*A*)	15.1	15.6
20,40	16,31	3.8 (*D*)	78.3	0.031	2.4 (*D*)	2.6	2.8
20,40	15,34	0.5 (*D*)	43.5	0.007	0.3 (*D*)	0.2	0.4
20,40	15,33	3.5 (*C*)	43.5	0.071	3.1 (*C*)	1.9	2.9
20,40	15,32	14.9 (*B*)	43.5	0.264	11.5 (*B*)	10.5	8.6
20,40	15,31	26.6 (*A*)	43.5	0.469	20.4 (*A*)	18.2	17.9
20,40	15,30	10.4 (*D*)	43.5	0.166	7.2 (*C*)	9.6	9.0
20,40	15,29	1.5 (*D*)	43.5	0.023	1.0 (*D*)	1.5	2.9
20,40	14,32	0.8 (*D*)	68.5	0.009	0.6 (*D*)	0.2	0.3
20,40	14,31	6.4 (*C*)	68.5	0.066	4.5 (*C*)	1.3	1.6
20,40	14,30	25.7 (*A*)	68.5	0.222	15.2 (*A*)	12.0	8.6
20,40	14,29	41.3 (*A*)	68.5	0.394	27.0 (*A*)	26.2	11.8
20,40	14,28	26.9 (*A*)	68.5	0.270	18.5 (*A*)	17.9	10.9
20,40	14,27	4.7 (*C*)	68.5	0.039	2.7 (*C*)	3.5	2.3
26,56	16,55	164.3 (*A*)	73.7	0.805	59.3 (*B*)	58.9	53.6
26,56	26,54	28.2 (*B*)	73.7	0.166	12.2 (*B*)	13.4	14.7
26,56	26,53	3.0 (*D*)	73.7	0.030	2.2 (*D*)	3.2	2.4
26,56	25,55	53.7 (*A*)	132.6	0.266	35.3 (*A*)	37.8	50.7
26,56	25,54	66.9 (*A*)	132.6	0.319	42.3 (*A*)	40.2	61.6
26,56	25,53	64.0 (*A*)	132.6	0.302	40.0 (*A*)	41.4	35.5
26,56	25,52	21.6 (*B*)	132.6	0.104	13.8 (*B*)	16.2	14.4
26,56	25,51	3.9 (*D*)	132.6	0.020	2.6 (*D*)	4.1	3.8
26,56	24,54	4.7 (*C*)	120.1	0.025	3.0 (*C*)	3.5	2.9
26,56	24,53	16.0 (*B*)	120.1	0.095	11.4 (*B*)	16.3	21.0
26,56	24,52	63.6 (*A*)	120.1	0.337	40.5 (*A*)	38.5	61.6
26,56	24,51	60.7 (*A*)	120.1	0.321	38.5 (*A*)	39.8	40.7
26,56	24,50	30.5 (*A*)	120.1	0.197	23.7 (*A*)	18.7	20.2
26,56	24,49	5.1 (*C*)	120.1	0.030	3.6 (*C*)	3.7	3.5
26,56	23,52	1.1 (*D*)	88.5	0.008	0.7 (*D*)	0.9	1.3
26,56	23,51	8.3 (*C*)	88.5	0.076	6.7 (*C*)	6.9	6.2
26,56	23,50	33.1 (*A*)	88.5	0.284	25.1 (*A*)	23.0	17.5
26,56	23,49	43.0 (*A*)	88.5	0.381	33.7 (*A*)	32.7	32.8
26,56	23,48	24.7 (*A*)	88.5	0.220	19.5 (*A*)	19.8	12.5
26,56	23,47	4.9 (*D*)	88.5	0.032	2.8 (*D*)	4.9	3.8

TABLE II. (*Continued*).

From Z, A	To Z, A	Carbon isotopic cross section (error)	Hydrogen charge cross section	Hydrogen mass fraction	Hydrogen isotopic cross section (error)	U.N.H. hydrogen calculations	T&S hydrogen calculations
26,56	22,50	1.6 (*D*)	85.6	0.014	1.2 (*D*)	0.8	2.4
26,56	22,49	8.4 (*C*)	85.6	0.082	7.0 (*C*)	6.5	6.5
26,56	22,48	30.5 (*A*)	85.6	0.261	22.3 (*A*)	22.9	24.0
26,56	22,47	40.6 (*A*)	85.6	0.375	32.1 (*A*)	31.5	28.0
26,56	22,46	23.3 (*A*)	85.6	0.229	19.6 (*A*)	18.6	17.9
26,56	22,45	4.0 (*D*)	85.6	0.036	3.1 (*D*)	4.5	3.4
26,56	22,44	0.6 (*D*)	85.6	0.008	0.7 (*D*)	0.4	0.9
26,56	21,48	0.3 (*D*)	59.7	0.003	0.2 (*D*)	0.2	0.8
26,56	21,47	2.7 (*D*)	59.7	0.034	2.0 (*C*)	2.2	3.8
26,56	21,46	12.8 (*B*)	59.7	0.191	11.4 (*B*)	10.9	9.6
26,56	21,45	28.3 (*A*)	59.7	0.405	24.2 (*A*)	22.1	22.4
26,56	21,44	21.5 (*A*)	59.7	0.288	17.2 (*B*)	17.9	10.9
26,56	21,43	6.9 (*C*)	59.7	0.072	4.3 (*C*)	5.9	3.6
26,56	21,45	2.7 (*D*)	54.1	0.028	1.5 (*D*)	1.5	1.8
26,56	20,44	10.6 (*B*)	54.1	0.148	8.0 (*C*)	8.8	8.2
26,56	20,43	22.6 (*A*)	54.1	0.360	19.5 (*A*)	20.5	13.0
26,56	20,42	22.0 (*A*)	54.1	0.342	18.5 (*A*)	18.5	14.1
26,56	20,41	10.9 (*C*)	54.1	0.124	6.7 (*C*)	6.5	3.1
26,56	20,40	1.3 (*D*)	54.1	0.009	0.5 (*D*)	0.9	0.8
26,56	19,44	0.7 (*D*)	27.8	0.014	0.4 (*D*)	0.1	0.2
26,56	19,43	2.8 (*D*)	27.8	0.068	1.9 (*D*)	0.7	1.0
26,56	19,42	8.1 (*C*)	27.8	0.201	5.6 (*C*)	4.5	3.1
26,56	19,41	16.6 (*B*)	27.8	0.367	10.2 (*B*)	10.7	9.2
26,56	19,40	14.6 (*B*)	27.8	0.237	6.6 (*C*)	9.7	8.2
26,56	19,39	7.3 (*C*)	27.8	0.097	2.7 (*D*)	3.3	3.2
26,56	19,38	1.0 (*D*)	27.8	0.018	0.5 (*D*)	0.4	0.6
26,56	18,41	1.7 (*D*)	24.9	0.020	0.5 (*D*)	0.4	0.5
26,56	18,40	8.0 (*C*)	24.9	0.124	3.1 (*C*)	2.8	2.6
26,56	18,39	17.9 (*B*)	24.9	0.301	7.5 (*B*)	9.0	5.2
26,56	18,38	19.1 (*B*)	24.9	0.390	9.7 (*B*)	10.5	10.0
26,56	18,37	6.1 (*C*)	24.9	0.120	3.0 (*D*)	4.2	2.7
26,56	18,36	1.1 (*D*)	24.9	0.044	1.1 (*D*)	0.7	0.9
26,56	17,39	0.9 (*D*)	16.6	0.012	0.2 (*D*)	0.1	0.2
26,56	17,38	3.4 (*D*)	16.6	0.066	1.1 (*D*)	0.8	3.3
26,56	17,37	12.5 (*B*)	16.6	0.265	4.4 (*C*)	4.1	4.8
26,56	17,36	13.5 (*B*)	16.6	0.380	6.3 (*C*)	7.1	2.5
26,56	17,35	9.6 (*C*)	16.6	0.259	4.3 (*C*)	4.4	0.5
26,56	17,34	0.9 (*D*)	16.6	0.018	0.3 (*D*)	0.9	0.1
26,56	16,37	0.6 (*D*)	18.1	0.011	0.2 (*D*)	0.1	0.1
26,56	16,36	2.2 (*D*)	18.1	0.050	0.9 (*D*)	0.5	0.9
26,56	16,35	8.0 (*C*)	18.1	0.177	3.2 (*C*)	3.6	2.0
26,56	16,34	14.6 (*B*)	18.1	0.337	6.1 (*C*)	7.6	5.6
26,56	16,33	11.1 (*B*)	18.1	0.276	5.0 (*C*)	5.2	2.2
26,56	16,32	5.6 (*C*)	18.1	0.116	2.1 (*D*)	1.3	0.8
26,56	16,31	1.6 (*D*)	18.1	0.033	0.6 (*D*)	0.2	0.1
28,58	28,57	164.5 (*A*)	64.9	0.846	54.9 (*B*)	50.0	40.4
28,58	28,56	28.0 (*B*)	64.9	0.154	10.0 (*C*)	11.5	3.1
28,58	27,57	72.1 (*A*)	119.5	0.537	64.2 (*A*)	60.1	51.7
28,58	27,56	60.3 (*A*)	119.5	0.423	50.5 (*A*)	45.6	39.9
28,58	27,55	6.6 (*C*)	119.5	0.039	4.7 (*C*)	10.7	35.5
28,58	26,56	32.1 (*A*)	110.4	0.236	26.1 (*A*)	26.4	28.2
28,58	26,55	74.6 (*A*)	110.4	0.559	61.7 (*A*)	44.1	64.8
28,58	26,54	24.8 (*A*)	110.4	0.184	20.3 (*B*)	29.2	38.8
28,58	26,53	3.0 (*D*)	110.4	0.022	2.4 (*D*)	8.9	7.6

TABLE III. Isotopic cross sections in helium targets at 600 MeV/nucleon. Errors: $A=\pm1.5\%$, $B=\pm3\%$, $C=\pm5\%$, and $D=\pm10\%$.

From Z, A	To Z, A	Helium charge cross section	Helium isotopic cross section (error)
6,12	6,11	48.3	46.2 (*A*)
6,12	6,10	48.3	2.1 (*D*)
6,12	5,11	75.2	45.1 (*A*)
6,12	5,10	75.2	30.1 (*A*)
6,12	4,10	20.9	4.2 (*C*)
6,12	4,9	20.9	5.0 (*C*)
6,12	4,7	20.9	11.7 (*B*)
7,14	7,13	11.4	10.5 (*B*)
7,14	7,12	11.4	0.9 (*D*)
7,14	6,13	116.4	11.1 (*B*)
7,14	6,12	116.4	83.9 (*A*)
7,14	6,11	116.4	19.8 (*A*)
7,14	6,10	116.4	1.6 (*D*)
7,14	5,11	46.2	26.0 (*A*)
7,14	5,10	46.2	20.2 (*A*)
7,14	4,10	24.9	3.1 (*D*)
7,14	4,9	24.9	4.4 (*D*)
7,14	4,7	24.9	17.4 (*B*)
8,16	8,15	53.4	50.3 (*A*)
8,16	8,14	53.4	3.1 (*D*)
8,16	7,15	90.3	45.7 (*A*)
8,16	7,14	90.3	37.8 (*A*)
8,16	7,13	90.3	6.8 (*C*)
8,16	6,14	98.3	3.5 (*C*)
8,16	6,13	98.3	26.6 (*A*)
8,16	6,12	98.3	50.6 (*A*)
8,16	6,11	98.3	15.8 (*B*)
8,16	6,10	98.3	1.8 (*D*)

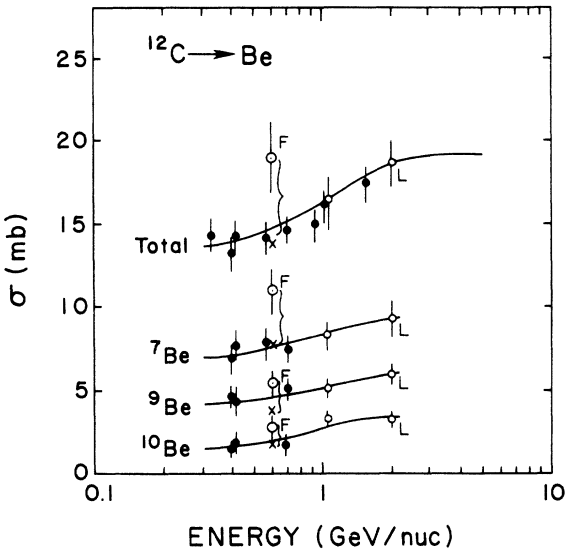

FIG. 4. Measurements of the cross sections for the reaction $^{12}C \rightarrow$ Be isotopes between 0.3 and 2.0 GeV/nucleon. Measurements by Lindstrom *et al.* (Ref. 3) (*L*) and Fontes (Ref. 13) (*F*) shown in addition to results from this study. Solid line is the cross section obtained from the new semiempirical formula presented in paper IV (Ref. 12).

IV. COMPARISON WITH OTHER DATA

The data presented in Tables II and III are the most comprehensive set of high-energy isotopic cross sections currently available in the literature. However, there is a large body of other data available in the literature with which to compare these new cross sections. In what follows, we shall compare our new cross sections with earlier ones for several cases of special interest. These include (1) $^{12}C \rightarrow$ Be, including the monitor cross section $^{12}C \rightarrow {}^{7}Be$, (2) $^{16}O \rightarrow N$, (3) $^{56}Fe \rightarrow$ Mn and Ar (of special interest for meteoritic studies), and (4) the monitor reactions $^{27}Al \rightarrow {}^{22}Na$ or ^{24}Na and other data on ^{22}Na and ^{24}Na production.

(1) $^{12}C \rightarrow$ Be. In Fig. 4 we show our measurements and others for the production of Be from ^{12}C in the energy range 0.3–2.0 GeV/nucleon. We have already discussed the Fontes *et al.*[13] measurement of the total cross section $^{12}C \rightarrow$ Be in paper II, in which we were able to reconcile his total cross sections to Be (and B) with ours in terms of the fact that he had used a different normalization to the monitor cross section $^{12}C \rightarrow {}^{7}Be$. It is evident that if his cross sections are reduced by $\sim 30\%$ for all Be isotopes, all of the data presented in Fig. 4 between 0.3–2.0 GeV/nucleon is in excellent agreement for all isotopes. Turning to the monitor cross section, we show in Fig. 5 a compilation of all of the available cross sections for $^{12}C \rightarrow$ Be as made originally by Cumming.[14] This figure predicts a cross section ~ 11.0 mb for the $^{12}C \rightarrow {}^{7}Be$ reaction at ~ 600 MeV/nucleon, the value adapted by Fontes *et al.*[13] To this figure we have added our new data and also that of Lindstrom *et al.*[3] The trend of all of this new data is for the cross sections to increase with increasing

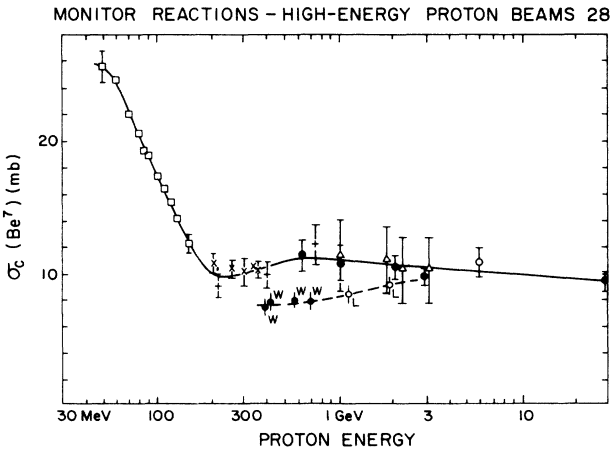

FIG. 5. Summary of measurements of the monitor cross section $^{12}C \rightarrow {}^{7}Be$ from Cumming (Ref. 14) and solid line fit to the data given in that paper. Measurements from this study shown as solid circles labeled *W*. Other new measurements labeled *L* indicated by same symbols as Fig. 4. Dashed line is a fit to these new measurements.

energy above a few hundred MeV/nucleon in contrast to earlier data that showed a broad peak in the region of a few hundred MeV/nucleon. The new data give a cross section for the $^{12}C \rightarrow {}^{7}Be$ reaction ~7.7 mb at 600 MeV/nucleon and this is the factor adapted to correct this and other Fontes *et al.*[13] measurements made at 600 MeV/nucleon.

We should note that a similar difference in magnitude and energy dependence is also observed between our results and earlier results for the $^{12}C \rightarrow {}^{11}C$ reaction (also summarized by Cumming[14]) and for the reaction involving $^{16}O \rightarrow {}^{15}O$ or ^{15}N.

(2) $^{16}O \rightarrow N$. In Fig. 6 we show a summary of measurements of the production of N from ^{16}O. In this case our measurements, in conjunction with those of Lindstrom *et al.*,[3] show an almost flat energy dependence above a few hundred MeV/nucleon, in contrast to earlier indications of a peak in this reaction at several hundred MeV/nucleon, as typified by the prediction of the semiempirical formula of Tsao and Silberberg,[10] shown as a dashed line in this figure. This difference and other differences in these cross sections, have played an important role in the recent conclusion that ^{14}N is strongly underabundant in the cosmic-ray sources—an important but not well understood indicator of the nucleosynthesis taking place in these sources (Webber and Gupta[17]).

(3) $^{56}Fe \rightarrow Mn$ or Ar. In Figs. 7 and 8 we show a summary of our measurements and others of the cross sections of two interesting products of ^{56}Fe fragmentation, Mn and Ar, above a few hundred MeV/nucleon. In these figures we also show our total elemental cross sections for ^{56}Fe into these two elements as presented in paper II. For Mn there is generally good agreement between our isotopic cross sections and those measured by Perron[18] and Orth *et al.*,[19]—after their individual isotopic cross sections are normalized to be equal to our measured total cross section of 132 mb for $^{56}Fe \rightarrow Mn$ at 600 MeV/nucleon. The dashed lines in Fig. 7 are drawn assuming a mass fraction for each isotope that is independent of energy. The agreement of the measurements with these curves, which is good over the energy range studied, indicates that the mass fractions have little or no energy dependence, a feature also observed for ^{12}C and ^{16}O fragmentation (see Sec. V C).

For the $^{56}Fe \rightarrow Ar$ isotopic cross sections shown in Fig. 8 the same format of data presentation is followed. The agreement of our data with that of Regnier[20] is good for ^{39}Ar, although for ^{38}Ar, the most abundant isotope, his values are ~20% higher than we measure. The isotopes ^{37}Ar and ^{40}Ar are not measured by Regnier, however,

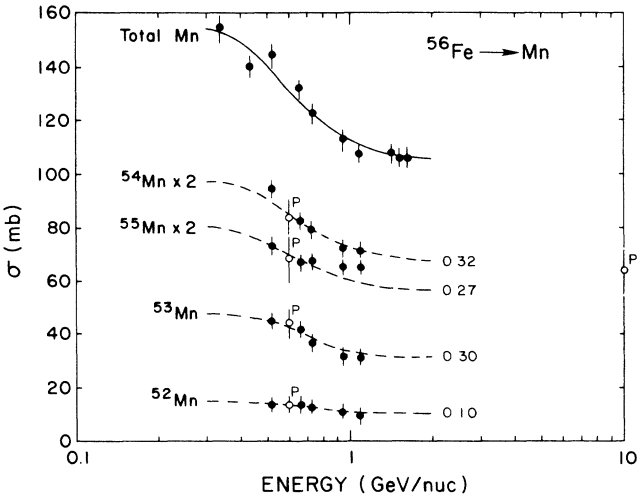

FIG. 7. Measurements of the cross section for the reaction $^{56}Fe \rightarrow Mn$ isotopes above 0.3 GeV/nucleon. Other measurements include Perron (Ref. 18) (*P*). Dashed lines represent mass fractions independent of energy as indicated.

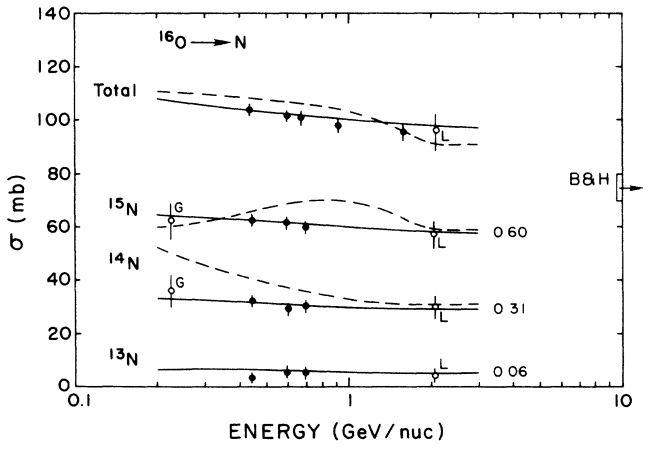

FIG. 6. Measurements of the cross section for the reaction $^{16}O \rightarrow N$ isotopes above 0.2 GeV/nucleon. Other new measurements include, Guzik *et al.* (Ref. 15) (*G*) and Brechtmann and Heinrich (Ref. 16) (*B* and *H*). Solid line is the cross section obtained from the new semiempirical formula presented in paper IV (Ref. 12). Dashed line is from Tsao and Silberberg (Ref. 10).

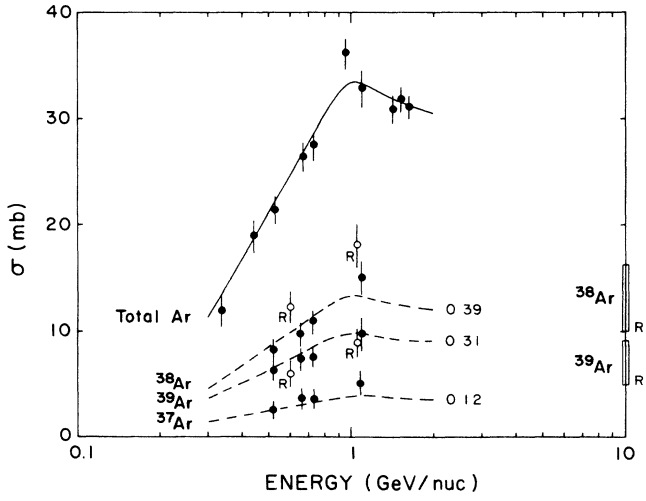

FIG. 8. Measurements of the cross section for the reaction $^{56}Fe \rightarrow Ar$ isotopes above 0.3 GeV/nucleon. Other measurements include Regnier (Ref. 20) (*R*). Dashed lines represent mass fractions independent of energy as indicated.

TABLE IV. Production of ^{22}Na, ^{24}Na and ^{26}Al (σ in mb). UNH denotes the University of New Hampshire.

		UNH				Other			
Energy (MeV/nucleon)	Parent	^{22}Na	^{24}Na	$^{22+24}$Na	^{26}Al	^{22}Na	^{24}Na	$^{22+24}$Na	^{26}Al
660/635	^{24}Mg	36.6				31.0[a]			
560/620	^{27}Al	9.6	11.4	21.0	36.5	14.5[a]	10.5[a]	25.0[a]	
770/300–600	^{28}Si	11.1	5.0	16.1	30.1	20.8[b,c]	4.7[b,c]	25.5[b,c]	22.5[d](±6)
649/300	^{32}S	10.5	3.1	13.6	13.9	9.1[b,c]	3.1[b,c]	12.2[b,c]	
656	^{40}Ar				2.1				

[a]Heydegger *et al.* (Ref. 22).
[b]Kirsten and Schaeffer (Ref. 21).
[c]Cumming (Ref. 14).
[d]Regnier (Ref. 20).

taking his mass fractions to be the same we measure, gives total elemental cross sections for ^{56}Fe→Ar of 26.5 and 39.5 mb at 600 and 1050 MeV/nucleon respectively, from the Regnier measurements, about 10% higher than we measure.

A considerable body of other data exists for the Fe→Ar reaction (e.g., Kirsten and Schaeffer[21]) since it is important for a number of cosmochemical problems related to meteorites. The ratio of the radioactive isotopes ^{37}Ar/^{39}Ar is particularly interesting for short term time variation studies. Our measured value for this ratio is 0.43±0.05.

(4) Another monitor reaction in wide usage is the reaction ^{27}Al→^{22}Na. A summary of measurements of this reaction is given in Fig. 9 from Cumming.[14] Note the large uncertainty in this reaction cross section above several hundred MeV/nucleon. Our value of 9.6 mb for this cross section at 600 MeV/nucleon is considerably below the value of 14.5 mb commonly adopted (e.g., Heydegger *et al.*[22]). However, our value taken in conjunction with the better known values of this cross section at higher energies shown in Fig. 9, shows a trend of almost flat or slightly decreasing cross sections below ~1 GeV/nucleon for this cross section similar to that observed for the ^{12}C→^{11}C and ^{12}C→^{7}Be reactions.

^{24}Na is also used as a monitor reaction. In Table IV, we show a summary of our measurements involving ^{22}Na, ^{24}Na, and ^{26}Al along with some other available measurements. Our value of 11.4 mb for the ^{27}Al→^{24}Na reaction cross section at 600 MeV/nucleon is consistent with the value ~11.0 mb given in the summary of Cumming[14] and the value of 10.5 mb measured by Heydegger *et al.*[22] In fact, the ^{22}Na cross section is commonly found from the ratio of intensities of the decay products of ^{22}Na and ^{24}Na. From our studies we find this ratio to be 0.84±0.09 at 600 MeV/nucleon. The fact that this ratio must be *less* than 1 also follows from our observation that the peak in the mass yield distribution for each of the secondary charge fragments from ^{27}Al fragmentation is always slightly larger than $2Z+1$ (see Table II and the following section discussing these mass yield distributions).

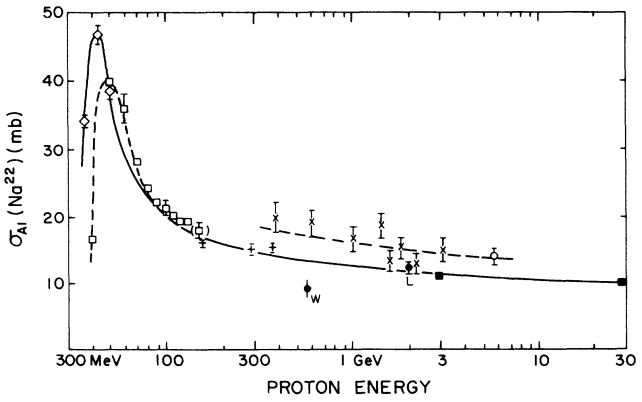

FIG. 9. Summary of measurements of the monitor cross section ^{27}Al→^{22}Na from Cumming (Ref. 14) including solid and dashed line fits to the data given in that paper. Measurement from this study at 600 MeV/nucleon shown as a solid circled labeled *W*.

V. SYSTEMATICS OF ISOTOPIC CROSS SECTIONS

The data set of isotopic cross sections we have presented in Tables II and III is perhaps the most comprehensive available for nuclei with $Z \leq 28$ incident on H, He, and C targets in terms of the number of different incident nuclei and the completeness of the mass yield distributions for each fragment charge. Most of the earlier measurements involved energetic proton beams incident on heavier targets and measured the cross sections for the production of mainly the individual radioactive isotope fragments. For protons incident on Fe, where the whole range of isotopes from $A=7-55$ is possible, there are perhaps ~20 useful radioactive isotopes available from this kind of study, however, many of these are far from the line of stability and have small cross sections. Perhaps 12 or so lie close enough to the line of stability or to the maximum in the mass yield distribution to have large enough cross sections so that the features of the mass yield distributions may be examined, but only a few secondary fragments such as Mn, Cr, Sc, and Ar have two or more useful radioactive isotopes. The systematics we wish to examine here are, in short, not easily accessible by the earlier techniques.

A. Ratio of isotopic cross sections in H, He, and C targets

In Figs. 10 and 11 we show the ratios of isotopic cross sections in H, He, and C targets as a function of the mass

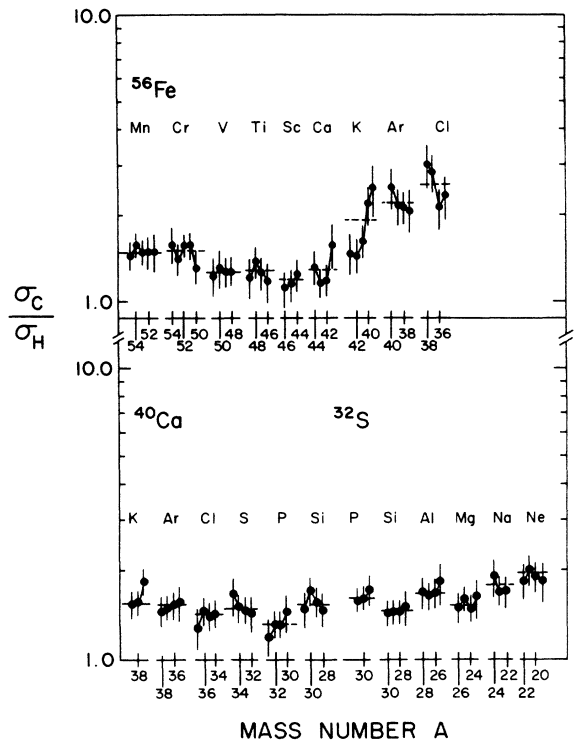

FIG. 10. Ratio of isotopic cross sections in H and C targets as a function of mass number A of the fragment for ^{56}Fe, ^{40}Ca, and ^{32}S beams. Dashed lines refer to average elemental cross section ratios for these targets.

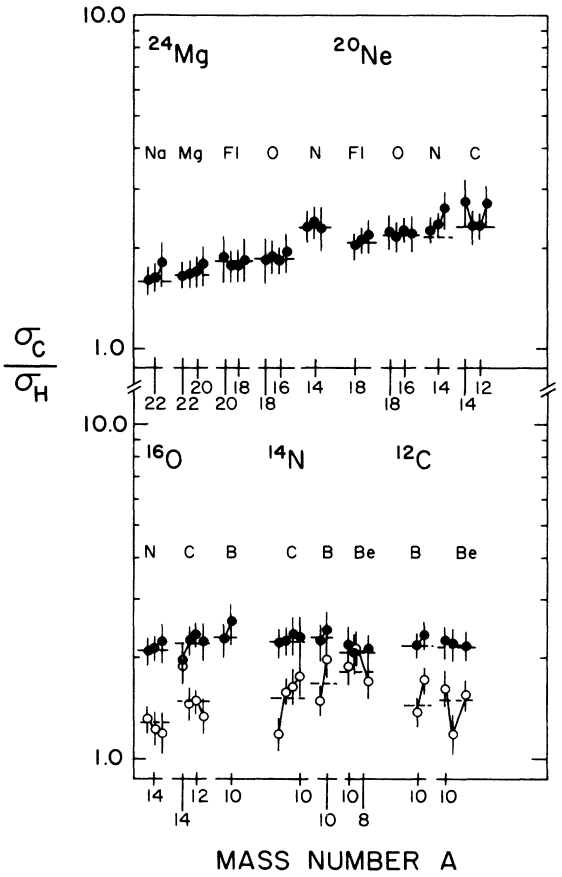

FIG. 11. Ratio of isotopic cross sections in H, He, and C targets as a function of mass number A of the fragment for ^{24}Mg, ^{20}Ne, ^{16}O, ^{14}N, and ^{12}C beams. Dashed lines refer to average elemental cross section ratios for these targets. He target data shown as open circles.

number of the fragment for incident ^{56}Fe, ^{40}Ca, ^{32}S, ^{24}Mg, ^{20}Ne, ^{16}O, ^{14}N, and ^{12}C beams (at an energy $\sim$600 MeV/nucleon). The average ratio for each charge is shown as a dashed line. The isotopic cross section ratios appear to be independent of the mass number of the fragment for each charge and are consistent with the average value determined for the charge changing cross section ratios for that charge. There is no clearly obvious systematic trend of the isotopic cross section ratios as a function of location on the mass yield curve, for example. This is a very important feature of the data that can be used for scaling the isotopic cross sections to different targets. It also means that the isotopic cross sections are subject to a very simple form of factorization in terms of the hydrogen target cross sections, σ^i_{BH},

$$\sigma^i_{Bt}=\gamma_{it}\sigma^i_{BH} ,$$

where the factor γ_{it} depends only on the target t. (Since the elemental ratios change as a function of energy, γ_{it} will also be a function of energy). Physically this implies that the fragmentation of a beam nucleus is independent of the complexity of the interaction, and depends only on the specific nucleus—target interaction.

B. Mass yield functions for hydrogen targets

In Figs. 12–14 we present the mass fraction distributions for the isotopic cross sections measured from ^{56}Fe, ^{40}Ca, ^{32}S, ^{24}Mg, ^{20}Ne, and ^{16}O beams incident on hydrogen targets. Note that, from the discussion just completed and the data shown in Figs. 10 and 11, the mass fraction distributions for He and C targets at the same energy should be similar.

Also shown in these figures are the mean mass of the fragments for each charge and the width, δ in u, of the mass distribution assuming it to be Gaussian. A very consistent pattern is followed for all mass distributions. The δ of the mass distribution depends essentially on the fragment charge Z_f and becomes narrower as the fragment charge becomes smaller. This is illustrated in Fig. 15, which shows δ as a function of Z_f for various beam charges.

The mean mass of the fragments, or equivalently the neutron excess, also behaves in a systematic and predictable fashion. This is shown in Fig. 16 in which the neutron excess of the peak of the mass distributions is plotted as a function of Z_f. Also shown in this figure is the line of β stability. As the difference Z_B-Z_f increases, the peak in the mass distribution moves rapidly from the neutron excess of the beam charge to a point close to, but generally slightly lower, than the line of β stability. Odd-even Z effects are evident, particularly at lower Z_f. Here the neutron excess of the even Z fragments is less

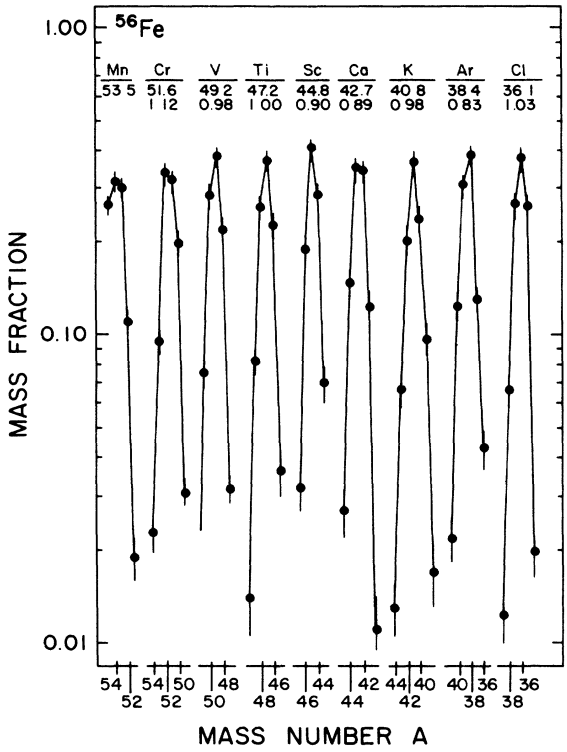

FIG. 12. Mass distributions of isotopic cross sections in hydrogen targets for fragments of ^{56}Fe interactions. Numbers under the fragment charge indicate (1) the mean A of the mass distribution and (2) width δ in u of the mass distribution.

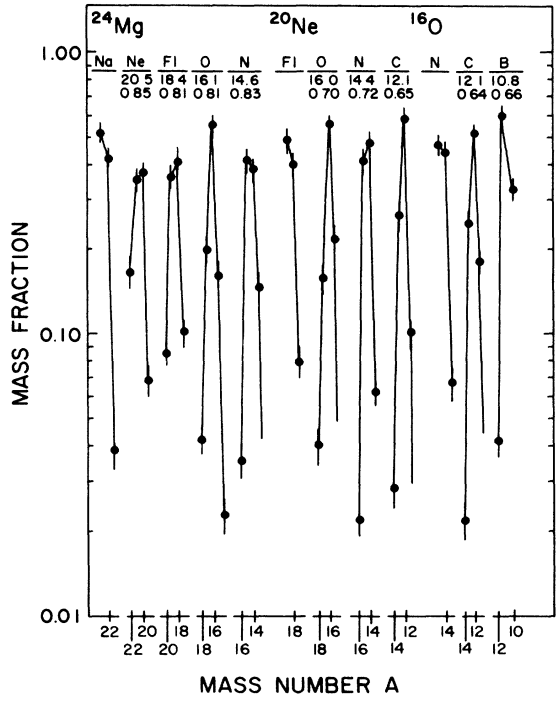

FIG. 14. Same as Fig. 12 but for ^{24}Mg, ^{20}Ne, and ^{16}O interactions.

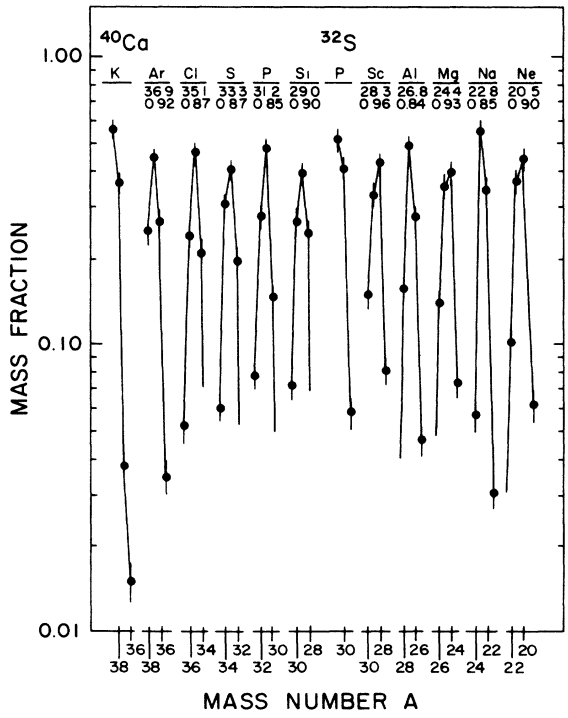

FIG. 13. Same as Fig. 12 but for ^{40}Ca and ^{32}S interactions.

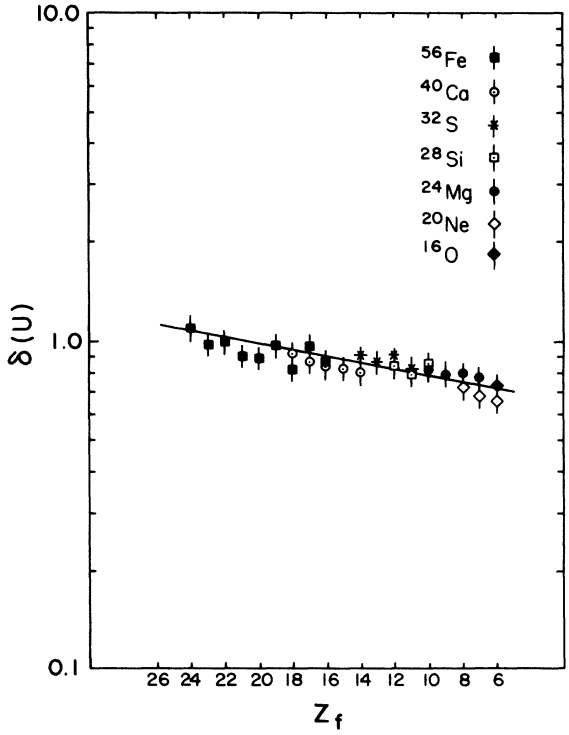

FIG. 15. The width, δ, of the mass distributions in hydrogen targets as a function of the fragment charge for various Z_B.

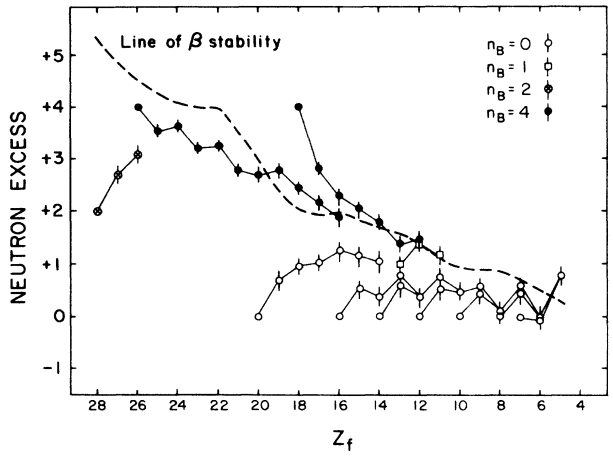

FIG. 16. The mean neutron excess of the mass distributions in hydrogen targets as a function of fragment charge for various Z_B, A_B. Also shown in the figure as a dashed line is the line of β stability.

than the odd Z fragments and, in fact, is ~zero for $Z_f = 6$ and 8.

These systematics are obviously important for understanding the fundamentals of the fragmentation process and also as a basis for an empirical derivation of a cross section formula as we will discuss in paper IV.

C. Energy dependence of the isotopic cross sections for hydrogen targets

The energy dependence of the isotopic cross sections is an important quantity that has been widely discussed in the literature. Two examples of this type of study for ^{56}Fe fragmentation are the work of Regnier[20] and Brodzinski *et al.*,[23] again for radioactive fragments only. We have already presented our extensive study of the energy dependence of the elemental cross sections in paper II. The question we now ask is—do the mass yield distributions change with energy? If these mass yield distributions are energy independent then, for each charge, the isotopic cross sections will have a similar energy dependence to that for the elemental cross sections presented in paper II. We have presented evidence in Figs. 7 and 8 of this paper that for ^{56}Fe→Mn and Ar, no strong energy dependence of the mass yields is observed between about 0.5–1.0 GeV/nucleon.

In Fig. 17 we show measured mass yield distributions for the additional reactions ^{56}Fe→Cr and Ca. For our data we show the average mass fractions from the two lower-energy and two higher-energy measurements (~600 and 1000 MeV/nucleon respectively). Also shown are the measurements of Perron[18] and Orth *et al.*[19] at 600 MeV/nucleon and 21 GeV/nucleon. Again no systematic variation of the mass fractions with energy is observed for these charges. In fact, except for the production of ^{44}Ca, all of the different measurements shown in this figure are in excellent agreement.

For ^{40}Ar fragmentation we have made isotopic measurements at 521 and 792 MeV/nucleon. These measurements may be compared with mass yield measurements

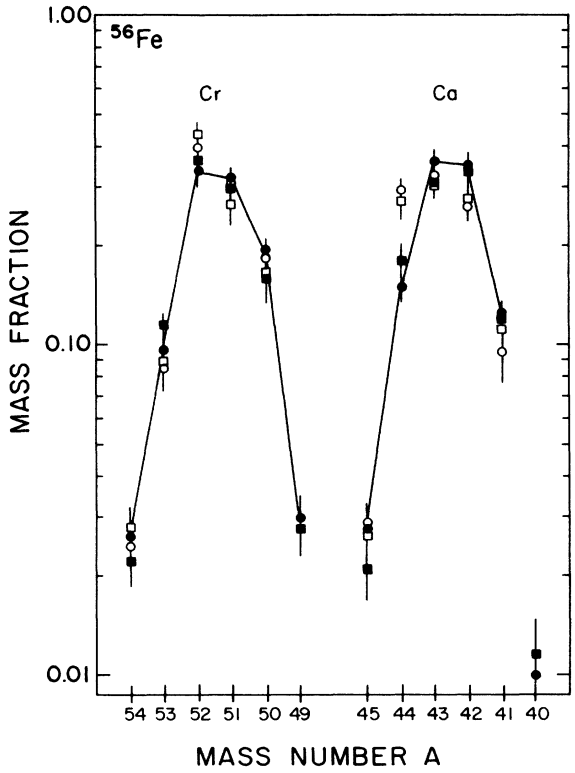

FIG. 17. Mass distributions of isotopic cross sections for the reactions ^{56}Fe→Cr and Ca isotopes. This data at ~0.6 GeV/nucleon, ●, and ~1.0 GeV/nucleon, ◇; Perron (Ref. 18) and Orth *et al.* (Ref. 19) at ~0.6 GeV/nucleon, ■, and ~21 GeV/nucleon, □.

from a CH_2 target reported by Lau[24] at an average target energy of 287 MeV/nucleon. We have used our direct measurements of mass yields from CH_2 targets and these are compared with the Lau data in Fig. 18. In general these mass yields are very similar for each charge over the energy range covered, except for one notable exception, involving $\Delta Z = 0$ and 1 fragments. For the $Z = 1$ fragment Cl, the production of the $A = 38$ and 39 isotopes clearly increases with energy, whereas for the Ar fragments themselves, the production of isotopes involving the loss of three and four neutrons is larger at lower energies.

For ^{16}O and ^{12}C fragmentation we may compare our measured mass fractions at ~600 MeV/nucleon with those measured by Lindstrom *et al.*[3] at 1.05 and 2.1 GeV/nucleon. This comparison is shown in Fig. 19. Again there is excellent agreement between the two data sets and no evidence of any significant energy dependence of the mass fractions.

Overall then we observe little evidence of any significant energy dependence of the mass fractions above a few hundred MeV/nucleon. This implies that the energy dependence of the isotopic cross sections is essentially the same for each charge as the charge changing cross sections presented in paper II. Exceptions to this behavior may occur at lower energies, particularly for neutron and proton stripping reactions as noted earlier.

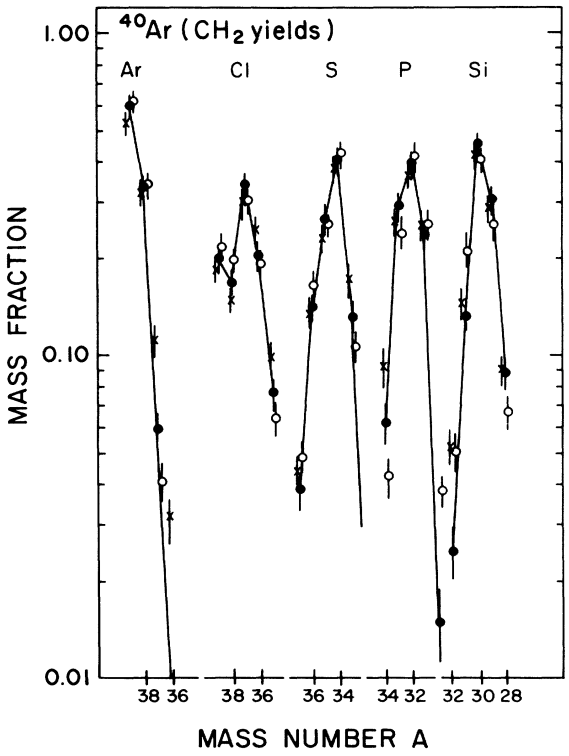

FIG. 18. Mass yields from CH_2 targets for ^{40}Ar fragmentation in this experiment, 521 MeV/nucleon, ●, and 792 MeV/nucleon, ϕ, and Lau (Ref. 24) at 287 MeV/nucleon, ✳.

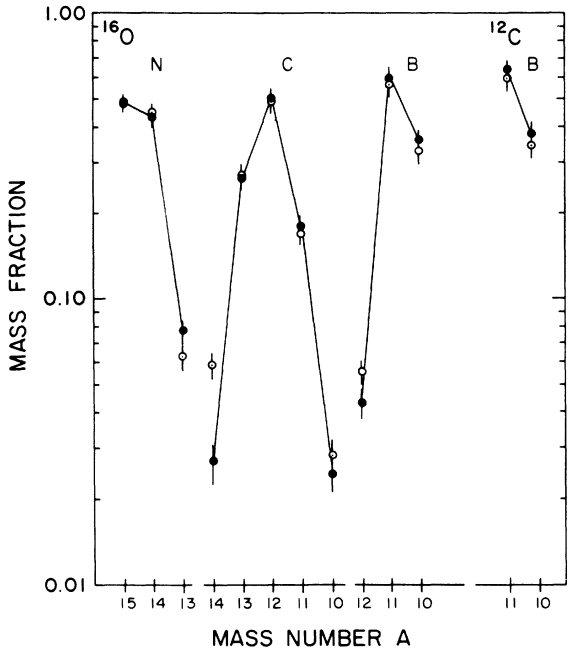

FIG. 19. Mass distributions of isotopic cross sections for fragments of ^{16}O and ^{12}C interactions in this experiment at ~0.6 GeV/nucleon, ●, and Lindstrom *et al.*,[3] at 1.05 and 2.1 GeV/nucleon, ϕ.

D. Neutron and proton stripping reactions

A considerable amount of new and interesting data has also been obtained on neutron and proton stripping reactions in this study. Some of this, related to the energy dependence of the total cross sections has already been discussed in paper I. Here, briefly, we would like to note some features of these stripping reactions at a fixed energy ~600 MeV/nucleon. Consider first nuclei with $A=2Z$ for which we have a nearly complete set of cross sections for even Z_B between 6 and 20. The neutron stripping cross sections for all of these reactions are ~30 mb; the proton stripping cross sections average $\sim 1.2x$, this, probably due to the fact that the fragment nucleus in this case is closer to the line of β stability. Exceptions to this behavior, for proton stripping, are ^{20}Ne→^{19}Fl, which is much less than the average, and ^{28}Si→^{27}Al, which is greater than the average. In both cases this is due to the stability of the fragments nucleus. We also observe that the $2p$ cross sections are always larger than the $2n$ cross sections for beam nuclei where $A=2Z$; in several cases, ^{24}Mg→^{22}Ne, ^{28}Si→^{26}Mg, ^{32}S→^{30}Si, and ^{40}Ca→^{38}Ar, they are up to a factor $\sim 10x$ larger, again because of the stability of the fragment nucleus.

For beam nuclei with a neutron excess, the neutron stripping cross sections are found to increase relative to the proton stripping cross sections, actually becoming a factor ~2 larger for the $1n$ reaction for beam charges with a neutron excess of 4, such as ^{56}Fe and ^{40}Ar. For these beam nuclei the cross sections for $1n$ and $2n$ stripping are much larger than the similar cross sections for beam nuclei with $A=2Z$ as well. All of these details of stripping reactions are consistent with behavior in which the cross sections depend on the stability of the fragment nucleus.

[1]W. R. Webber, J. C. Kish, and D. A. Schrier, Phys. Rev. C **41**, 520 (1990), this issue.
[2]W. R. Webber, J. C. Kish, and D. A. Schrier, Phys. Rev. C **41**, 533 (1990), the preceding paper.
[3]P. J. Lindstrom, D. E. Greiner, H. H. Heckman, B. Cork, and F. S. Bieser, Lawrence Berkeley Laboratory Report No. 3650, 1975 (unpublished).
[4]D. L. Olsen, B. L. Berman, D. E. Greiner, H. H. Heckman, P. J. Lindstrom, and H. J. Crawford, Phys. Rev. C **28**, 1602 (1983).
[5]D. E. Greiner, P. J. Lindstrom, H. H. Heckman, B. Cork, and F. S. Bieser, Phys. Rev. Lett. **35**, 152 (1975).
[6]H. H. Heckman, D. E. Greiner, P. J. Lindstrom, and F. S. Bieser, Phys. Rev. Lett. **28**, 926 (1972).
[7]W. R. Webber, J. A. Lezniak, and J. C. Kish, Astrophys. J. **183**, L81 (1973).

[8]W. R. Webber, Astrophys. J. **252**, 386 (1982).
[9]J. S. Young, P. S. Frier, C. J. Waddington, N. R. Brewster, and R. K. Fickle, Astrophys. J. **246**, 1014 (1981).
[10]C. H. Tsao and S. Silberberg, Proc. 16th ICRC **2**, 202 (1979).
[11]W. R. Webber, Proc. 20th ICRC **8**, 65 (1987).
[12]W. R. Webber, J. C. Kish, and D. A. Schrier, Phys. Rev. C **41**, 566 (1990), the following paper.
[13]P. Fontes, C. Perron, J. Lestringuez, F. Yiou, and R. Bernas, Nucl. Phys. **165**, 405 (1971).
[14]J. B. Cumming, Annu. Rev. Nucl. Sci. **13**, 261 (1963).
[15]T. G. Guzik, J. P. Weferl, H. J. Crawford, D. E. Greiner, P. J. Lindstrom, W. Schimmerling, and T. M. J. Symons, Proc. 19th ICRC **2**, 80 (1985).
[16]C. Brechtmann and W. E. Heinrich, Z. Phys. (in press).
[17]M. Gupta and W. R. Webber, Astrophys. J. **340**, 1124 (1989).
[18]C. Perron, Phys. Rev. C **14**, 1108 (1976).
[19]C. J. Orth, H. A. Obren, M. E. Schillaci, B. J. Dropesky, J. E. Cline, E. B. Nieschmidt, and R. L. Brodzinski, J. Inorg. Nucl. Chem. **38**, 13 (1976).
[20]S. Regnier, Phys. Rev. C **20**, 1517 (1979).
[21]T. A. Kirsten and O. A. Schaeffer, *Interactions of Elementary Particles, Research in Science and Technology,* edited by L. C. L. Yuan (Academic, New York, 1962), p. 14.
[22]H. R. Heydegger, A. L. Turkevich, A. Van Ginnekan, and P. H. Walpole, Phys. Rev. C **14**, 1506 (1976).
[23]R. L. Brodzinski, L. A. Rancitelli, J. A. Cooper, and N. A. Wogman, Phys. Rev. C **4**, 1257 (1971).
[24]K. Lau, Ph.D. thesis, California Institute of Technology, 1985.